IEEE Access
Multidisciplinary | Rapid Review | Open Access Journal

Received 2 December 2023, accepted 22 December 2023, date of publication 8 January 2024,
date of current version 17 January 2024.

Digital Object Identifier 10.1109/ACCESS.2024.3351174

RESEARCH ARTICLE

Analysis of Cogging Torque of Permanent Magnet Motors Under Mixed-Eccentricity and Manufacturing Tolerances

YUE ZHAO[1], SHUO ZHANG[1], (Member, IEEE), CHENGNING ZHANG[1], GUOHUI YANG[2], AND YONGXI YANG[1]

[1]School of Mechanical and Vehicle Engineering, Beijing Institute of Technology, Beijing 100811, China
[2]Laboratory of Aerospace Servo Actuation and Transmission, Beijing Institute of Precision Mechatronics and Controls, Beijing 100076, China

Corresponding author: Yongxi Yang (yongxi.yang2018@gmail.com)

The work was supported by the National Key Research and Development Program of China, under Grant 2022YFB2502703.

ABSTRACT The rotor eccentricity and manufacturing tolerances caused by unavoidable uncertainties in the process of manufacturing deteriorate the cogging torque of permanent magnet (PM) motors. To guide the design and optimization of PM motors, this paper proposes an analytical model to reveal the effects of mixed-eccentricity (ME) and manufacturing tolerances on the harmonic components of cogging torque. A coefficient is introduced to intuitively characterize the impact of ME on the distribution of the air-gap length. Then a modified analytical model is developed to theoretically identify the additional harmonic components (AHCs) of cogging torque associated with the eccentricity and tolerances. And the main AHCs of cogging torque are quantitatively determined through the finite element method. Finally, suggestions to improve the robustness considering uncertainties by selecting pole/slot combination and pole-arc ratio are proposed.

INDEX TERMS Permanent magnet motors, mixed-eccentricity (ME), manufacturing tolerances, additional harmonic components (AHCs) of cogging torque, robust design.

I. INTRODUCTION

The permanent magnet (PM) motor has been widely used in domestic and industrial applications due to its advantages such as wide speed range and high power density [1]. However, the cogging torque of PM motors, caused by the interaction between the rotor magnets and the slotted stator, is one of the sources of torque ripple and affects the output accuracy [2].

To reduce the cogging torque, several methods have been proposed to eliminate the inherent harmonic components of cogging torque, including the optimization pole-arc coefficient [3], skewing [4], unequal/asymmetrical magnet widths [5], harmonic currents injection [6], and so on. However, due to the unavoidable uncertainties in the process of manufacturing and assembling, rotor eccentricity and manufacturing tolerances are frequently present, and the additional harmonic components (AHCs) of cogging torque might be introduced in practical motors [7], [8], [9].

Rotor eccentricity refers to as the phenomenon that the center of the rotor does not coincide with the center of the stator. Eccentricity can be categorized into three types based on the rotation center of the rotor. Most existing studies on cogging torque under eccentricity have only examined static-eccentricity(SE) and dynamic-eccentricity (DE), i.e., the rotor rotates around the stator or rotor center. Zhu et al. [10] analyzed the cogging torque harmonics of different pole/slot configurations under SE and DE via the analytical approach and finite element method (FEM). The AHCs of cogging torque with multiples of the number of poles ($2p$) and slots (Q_s) orders can be introduced under SE and DE, respectively. The value of cogging torque under eccentricity when the rotor is fixed in one certain position could be analytically calculated by the coordinate transformations model [11] and

The associate editor coordinating the review of this manuscript and approving it for publication was Kan Liu.

© 2024 The Authors. This work is licensed under a Creative Commons Attribution-NonCommercial-NoDerivatives 4.0 License.
For more information, see https://creativecommons.org/licenses/by-nc-nd/4.0/

the subdomain model [12]. And the cogging torque wave could then be obtained once the rotor trajectory is known.

However, the mixed-eccentricity (ME), whose rotation center is neither the stator center nor the rotor center, is the more general case that is commonly encountered in practical applications [13]. Presently, the air-gap model for ME is usually written as the sum of SE and DE. Based on this model, the influence of ME on the radial force of PM motors [14], the dynamical model of induction motors under ME [15] and the influence of ME on air-gap flux density of PM motors [16] were analyzed. Yet the application of this model relies on a complex analysis process, where the influence of ME on cogging torque harmonic components could not be comprehensively explained.

The manufacturing tolerances typically refer to the uncertainties in the dimensions of stator teeth and rotor, and remanence tolerances on PMs. Ou et al. [8] conducted a systematic analysis of the influence of stator and rotor tolerances on cogging torque components, and proposed that stator and rotor tolerances respectively result in multiples of $2p$ and Q_s orders AHCs of cogging torque. Yang et al. [17] provided suggestions for selecting various design parameters to eliminate the AHCs of cogging torque and reduce the effects of manufacturing tolerances. However, in practical motors, the rotor eccentricity and manufacturing tolerances may coexist and have a coupled influence. Galfarsoro et al. [18] proved that the manufacturing tolerances together with SE and DE would have additional effects beyond their independent influences. Therefore, solely focusing on one of these factors in the uncertainty analysis of cogging torque is inadequate and also does not conform to practice. However, no papers that systematically study the coupling mechanism of ME and manufacturing tolerances on the cogging torque of PM motors are found.

The objective of this paper is to analyze and summarize the main AHCs of cogging torque in PM motors introduced by ME and manufacturing tolerances simultaneously via a modified analytical model together with FEM. Consequently, the main AHCs of one PM motor having any pole/slot configurations under manufacturing uncertainties can be easily determined. This intuitive approach is substantially applicable to the robust design of PM motors and directional eliminating the influences of manufacturing uncertainties.

The remainder of this paper is organized as follows. The influence of ME on the permeance of air-gap is described and a coefficient is introduced to characterize the cogging torque harmonics under ME intuitively in Section II. Subsequently, Section III theoretically discusses the harmonic components of cogging torque in the PM motor under ME without/with manufacturing tolerances. And several PM motors with different pole/slot configurations are taken as examples to verify the efficacy of theoretical results through FEM and the main AHCs of cogging torque are revealed considering the coexistence of ME and manufacturing tolerances in Section IV. Finally, suggestions to improve the robustness considering manufacturing uncertainties are proposed in Section V.

II. THE ANALYTICAL MODEL OF COGGING TORQUE

The energy method is selected as the basic model in this paper to predict the harmonic components of cogging torque. This method can meet the requirement of the influence mechanism analysis of manufacturing uncertainties on cogging torque, though it has low precision in amplitude [8], [19]. The quantitative analysis is conducted later by the FEM.

A. PERMEABILITY OF AIR-GAP WITH ME

The schematic diagram of ME is shown in Fig. 1, where the outer circle presents the inner circle of the stator and the dotted inner circle represents the rotor in a healthy state. The inner circle of the solid line is the position of the rotor with eccentricity. The solid inner circle represents the position of the rotor with eccentricity. In this case, the rotor rotates around a point O that is neither the center of the rotor nor the stator, and the real motion trajectory of the center of the rotor is shown as the blue line in Fig. 1.

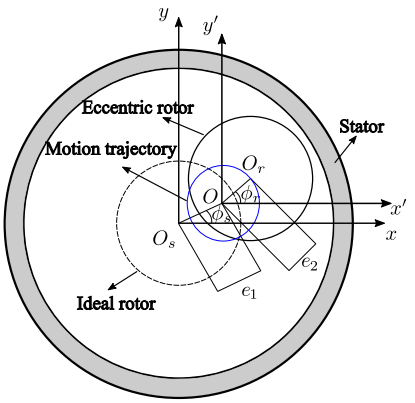

FIGURE 1. The schematic diagram of ME.

The motion process of the rotor with ME can be decoupled in two process. Firstly, as shown in Fig. 1, the center of the rotor and the rotating center deviate from the center of stator O_s to the point O. The distance between O_s and O is named as SE distance and represented by e_1. At this moment, the air-gap length can be formulated as [20]:

$$g_1(\theta) \approx \frac{g}{E_s(\theta - \phi_s)},$$
$$E_s(\theta - \phi_s) = \frac{1}{1 - \epsilon_1 \cos(\theta - \phi_s)}, \tag{1}$$

where θ is the angle in the stator reference frame, ϕ_s is the relative SE angle in the stator reference frame, g represents the air-gap length in the ideal condition, and SE ratio $\epsilon_1 = e_1/g$.

Then the center of rotor O_r deviate from rotating center O. The distance between O and O_r is named as DE distance and represented by e_2. But the rotor still rotates around point O, which is not concentric with O_s or O_r. In this case, the air-gap

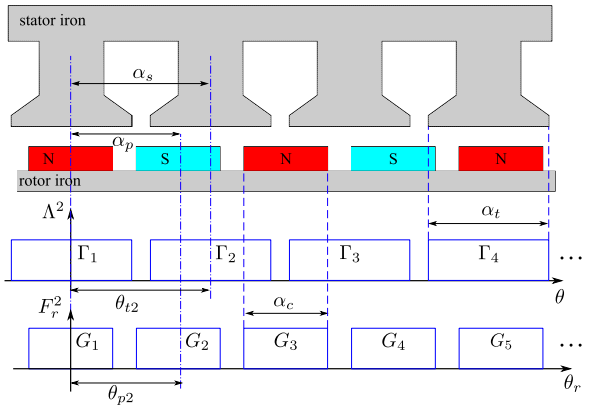

FIGURE 2. Equivalent rectangular waves of the squares of rotor MMF and permeance.

length can be formulated as:

$$g(\theta,\theta_r) \approx \frac{g_1(\theta)}{E_d(\theta_r-\phi_r)} = \frac{g(\theta)}{E_s(\theta-\phi_s)E_d(\theta_r-\phi_r)},$$
$$E_d(\theta_r-\phi_r) = \frac{1}{1-\epsilon_2\cos(\theta_r-\phi_r)}, \tag{2}$$

where θ_r is the angle in the rotor reference frame, ϕ_r is the relative DE angle in the rotor reference frame, and DE ratio $\epsilon_2 = e_2/g$.

Thus, the final relative permeability under ME can be calculated as:

$$\Lambda_m(\theta,\theta_r) = \Lambda E_m(\theta,\theta_r),$$
$$E_m(\theta,\theta_r) = E_s(\theta-\phi_s)E_d(\theta_r-\phi_r), \tag{3}$$

where Λ represents the relative permeability in the ideal condition, and $\Lambda = 1/g$.

Actually, the SE and DE correspond to the cases where only $\epsilon_2 = 0$ and only $\epsilon_1 = 0$, respectively. Therefore, the equivalent effect of ME on the air-gap could be regarded as the product of the independent effects of SE and DE on the air-gap.

B. THE ANALYTICAL MODEL OF COGGING TORQUE

According to the energy method, the cogging torque of PM motors is approximately generated by the energy variation within the air-gap. Based on the magnetic motive force (MMF)-Permeance model, the cogging torque under ME can be expressed as:

$$T_{cog}(\theta_m) = -\frac{\partial W}{\partial \theta_m}$$
$$= -K\frac{\partial}{\partial\theta_m}\int_0^{2\pi} F_r^2(\theta,\theta_m)\Lambda^2(\theta)E_m^2(\theta,\theta_m)d\theta,$$
$$K = \frac{L}{4\mu_0}\left(R_o^2 - R_i^2\right), \tag{4}$$

where F_r and Λ are the MMF of the rotor excited by PMs without consideration of the influence of slot-opening and the permeability of air-gap respectively. L is the active length of the motor; R_o and R_i are the outer and inner radii of the air gap, respectively. θ_m indicates the rotor position in the stator reference frame, and $\theta_m = \theta - \theta_r$.

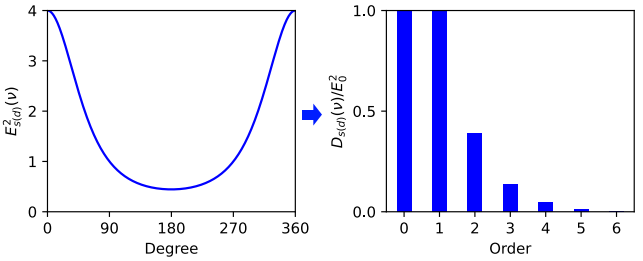

FIGURE 3. The normalized amplitude of E_s^2 and E_d^2 harmonics.

Assuming infinite permeability of iron and ignoring flux leakages, the square of rotor MMF and permeance of air-gap can be recognized as equivalent rectangular waves shown in Fig.2 and rewritten in the Fourier series in (5) [21].

$$F_r^2(\theta,\theta_m) = F_{r0}^2 + \sum_n G(n)\cos(n\theta - n\theta_m),$$
$$\Lambda^2(\theta,\theta_m) = \Lambda_0^2 + \sum_k \Gamma(k)\cos(k\theta), \tag{5}$$

where F_{r0}^2 and Λ_0^2 are constants, while $G(n)$ and $\Gamma(k)$ represent the amplitudes of the n^{th} and k^{th} harmonics, respectively.

$$G(n) = \sum_{i=1}^{2p}\frac{2G_i}{n}\sin\frac{n\pi a_c}{2p}e^{-jn\theta_{pi}},$$
$$\Gamma(k) = \sum_{i=1}^{Q_s}\frac{2\Gamma_i}{k}\sin\frac{k\pi a_t}{Q_s}e^{-jk\theta_{ti}}, \tag{6}$$

where G_i represents the amplitude of the F_r^2 wave of the i^{th} PM, and it is proportional to the square of remanenc. While Γ_i represents the amplitude of the Λ^2 wave of the i^{th} tooth, and it is inversely proportional to the square of air-gap length. $a_c = \alpha_c/\alpha_p$ and $a_t = \alpha_t/\alpha_s$ are the pole-arc ratio and tooth width ratio respectively, and θ_{pi} and θ_{ti} are the center positions of each pole and tooth respectively.

C. THE ME COEFFICIENT

As for the term $E_m^2(\theta,\theta_m)$ in (4), since it can be used to describe the influence of ME in cogging torque, it is defined as ME coefficient (MEC). According to (3), MEC is the product of E_s^2 and E_d^2, which can be can be expressed using the Fourier series as shown in (7).

$$E_m^2(\theta,\theta_m) = E_s^2(\theta-\phi_s)E_d^2(\theta-\theta_m-\phi_r),$$
$$E_s^2(\theta-\phi_s) = E_{s0}^2 + \sum_\nu D_s(\nu)\cos(\nu\theta - \nu\phi_s),$$
$$E_d^2(\theta-\theta_m-\phi_r) = E_{d0}^2 + \sum_\nu D_d(\nu)\cos(\nu\theta - \nu\theta_m - \nu\phi_r). \tag{7}$$

Considering the eccentricity ratio of practical PM motors is usually not too large, so only the case of $\epsilon_1 + \epsilon_2 \leq 0.5$ is

taken into account in this paper. When ϵ_1 or $\epsilon_2 = 0.5$, the normalized amplitude of E_s^2 and E_d^2 harmonics are expressed as $D_{s(d)}(\nu)/E_0^2$ in Fig. 3. Since the amplitudes are small when the order is more than 2^{nd}, only the constant term, 1^{st} and 2^{nd} harmonics are considered in the subsequent analysis. Therefore, the MEC can be expanded as (8).

$$\begin{aligned} E_m^2(\theta,\theta_m) &= E_{s0}^2E_{d0}^2 + A + B + C \\ A &= E_{d0}^2\sum_{\nu_1} D_s(\nu_1)\cos(\nu_1\theta - \nu_1\phi_s) \\ B &= E_{s0}^2\sum_{\nu_2} D_d(\nu_2)\cos(\nu_2\theta - \nu_2\theta_m - \nu_2\phi_r) \\ C &= \frac{1}{2}\sum_{\nu_1,\nu_2} D_s(\nu_1)D_d(\nu_2) \\ &\quad \cdot\cos[(\nu_1 \pm \nu_2)\theta \mp \nu_2\theta_m - (\nu_1\phi_s \pm \nu_2\phi_r)]. \end{aligned} \tag{8}$$

where $\nu_1 = 1{,}2$, and $\nu_2 = 1{,}2$. As can be observed in (8), there are four terms in the MEC. They are constant term $E_{s0}^2E_{d0}^2$, the trigonometric term A, B and C.

Significantly, the specific values of the eccentricity angle mainly affect the phases of torque harmonics rather than harmonic components [22]. To simplify the analysis process, the special case of $\phi_s = \phi_r = 0$ is taken as the example to analyze and the MEC can be rewritten as follows:

$$E_m^2(\theta,\theta_m) = E_{m0}^2 + \sum_{\mu_1}\sum_{\mu_2} D_m(\mu_1,\mu_2)\cos(\mu_1\theta - \mu_2\theta_m), \tag{9}$$

where the E_{m0}^2 is equal to the constant term in (8) and the trigonometric term is the sum of A, B and C in (8). Therefore, μ_1 is taken as the coefficients of θ in A, B and C, i.e., ν_1, ν_2, and $\nu_1 \pm \nu_2$, respectively. μ_2 is equal to the coefficients of corresponding θ_m, and $D_m(\mu_1,\mu_2)$ is the amplitude of corresponding harmonic component. Ignoring the products of higher-order terms, the main combinations of μ_1 and μ_2 are listed in Table 1.

TABLE 1. The main combinations of μ_1 and μ_2.

μ_1	0	1	2	3
μ_2	1	0, ±1, 2	0, 1, 2	1, 2

Actually, (9) can be seen as the common expression for different eccentricity cases. It represents the eccentricity coefficient of SE, when (μ_1,μ_2) is equal to (1,0) and (2,0), i.e., only e_1 is non-zero. While (μ_1,μ_2) is equal to (1,1) and (2,2), (9) is the eccentricity coefficient of DE, i.e., only e_2 is not equal to 0.

III. THEORETICAL ANALYSIS OF AHCS OF COGGING TORQUE

A. COGGING TORQUE UNDER ME

By substituting (5) and (9) to (4), considering prosthaphaeresis formulas and the character of trigonometric function integration, the cogging torque under eccentricity is:

$$\begin{aligned} T_{cog}(\theta_m) &= -K\frac{\partial}{\partial\theta_m}\int_0^{2\pi} F_r^2(\theta,\theta_m)\Lambda^2(\theta)E_m^2(\theta,\theta_m)d\theta \\ &= -K\frac{\partial}{\partial\theta_m}(\mathbb{A}+\mathbb{B}+\mathbb{C}+\mathbb{D}+\mathbb{E}), \\ \mathbb{A} &= T_A\int_0^{2\pi}\sum_{\mu_1,\mu_2} D_m(\mu_1,\mu_2)\cos(\mu_1\theta - \mu_2\theta_m)d\theta, \\ \mathbb{B} &= T_B\int_0^{2\pi}\sum_n\sum_k G(n)\Gamma(k)\cos[(n-k)\theta - n\theta_m]d\theta, \\ \mathbb{C} &= T_C\int_0^{2\pi}\sum_k\sum_{\mu_1,\mu_2}\Gamma(k)D_m(\mu_1,\mu_2) \\ &\quad \cdot\cos[(k-\mu_1)\theta - \mu_2\theta_m]d\theta, \\ \mathbb{D} &= T_D\int_0^{2\pi}\sum_n\sum_{\mu_1,\mu_2} G(n)D_m(\mu_1,\mu_2) \\ &\quad \cdot\cos[(n-\mu_1)\theta - (n-\mu_2)\theta_m]d\theta, \\ \mathbb{E} &= T_E\int_0^{2\pi}\sum_n\sum_k\sum_{\mu_1,\mu_2} G(n)\Gamma(k)D_m(\mu_1,\mu_2) \\ &\quad \cdot\cos[(n-k\pm\mu_1)\theta - (n\pm\mu_2)\theta_m]d\theta, \end{aligned} \tag{10}$$

where $\mathbb{A}$ to $\mathbb{E}$ are the terms of the energy within the air-gap that may contribute to the cogging torque under eccentricity, and the T_A to T_E are positive constants that are deemed irrelevant to the present study. According to (6), when manufacturing tolerances on PMs or slots are absent, the n and k are only equal to $2ip$ and iQ_s ($i = 1, 2, 3,\ldots$) respectively. In this section, the cogging torque performances are analyzed only under rotor ME without considering manufacturing tolerances on PMs or teeth.

Firstly, $\mathbb{A}$ is caused by the interaction of the constant terms of F_r^2 and Λ^2 and the trigonometric term of MEC. It is non-zero only when $(\mu_1,\mu_2)\in\{(0,1)\}$, that is, ME may introduce 1^{st} torque harmonic. However, it should be noted that cogging torque is the differential of energy, as demonstrated in equation (4), so that the amplitudes of cogging torque harmonics are multiples of the corresponding orders of the amplitudes of energy harmonics. Additionally, the amplitudes of the eccentricity ratio are not excessively large. Hence, the 1^{st} cogging torque harmonic may be considerably smaller than other harmonics with higher orders, rendering it negligible in practical applications.

Furthermore, $\mathbb{B}$ is due to the interaction of the trigonometric terms of F_r^2 and Λ^2 and the constant term of MEC. The harmonic components of $\mathbb{B}$ remain the same as the case without rotor eccentricity, namely, $iLCM(2p, Q_s)^{th}$ (the common multiples of $2p$ and Q_s).

Additionally, $\mathbb{C}$ is resulted from the interaction of the trigonometric terms of Λ^2 and MEC and the constant term of F_r^2, while $\mathbb{D}$ is caused by the interaction of the trigonometric terms of F_r^2 and MEC and the constant term of Λ^2. Since the numbers of the poles and slots of the motor widely used in practice are usually greater than 3 and μ_1 is no more

TABLE 2. The Possible orders of Cogging Torque Harmonics under ME ($n = 2i_1p$, $k = i_2Q_s$, i_1 and i_2 are both positive integers).

	$n > k$	$n < k$
$\lvert n-k\rvert = 0$	$iLCM(n,k)$,$iLCM(n,k) \pm 1$	
$\lvert n-k\rvert = 1$	$k-1$,k,n,$n+1$	$n-1$,n,k,$k+1$
$\lvert n-k\rvert = 2$	k,$n-1$,n	n,$n+1$,k
$\lvert n-k\rvert = 3$	k,$k+1$,$n-1$,n	n,$n+1$,$k-1$,k

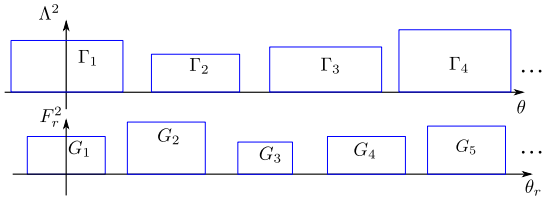

FIGURE 4. Equivalent rectangular waves of the squares of rotor MMF and permeance with manufacturing tolerances.

than 3, $\mathbb{C}$ and $\mathbb{D}$ can be ignored when only considering rotor eccentricity.

Finally, as for the $\mathbb{E}$, it is introduced by the interaction of the trigonometric terms of Λ^2, F_r^2, and MEC. $\mathbb{E}$ is non-zero only if $(n - k \pm \mu_1)$ is equal to 0. Thus, when n differs from k by no more than 3 and $(\mu_1, \mu_2) \in \{(1,0), (2,0), (1,1), (2,2)\}$, both n^{th} and k^{th} AHCs of cogging torque would be introduced simultaneously. Additionally, the extra AHCs with the middle orders of the most approximate n^{th} and k^{th} harmonics will also be introduced when $(\mu_1, \mu_2) \in \{(2,1), (3,1), (3,2)\}$. Notably, when the difference value of n and k is equal to 1, the AHCs with the nearest neighbor orders of n^{th} and k^{th} harmonics would be introduced because $(\mu_1, \mu_2) \in \{(1,-1), (1,2)\}$. And the harmonics of the $[iLCM(2p, Q_s) \pm 1]^{th}$ also exist because $(\mu_1, \mu_2) \in \{(0,1)\}$, when n is equal to k.

In conclusion, all possible harmonics of cogging torque under ME are listed in Table 2, in which the introduced harmonics of the row of "$|n-k| = 0$" are inherent additional cogging torque harmonics under ME no matter what pole/slot configurations.

Specially, as demonstrated in Section II, (μ_1, μ_2) in MEC is only equal to (1,0) and (2,0) when SE exists independently. According to $\mathbb{E}$ in (10), the n^{th} AHCs of cogging torque would be introduced in this case when n differs from k by no more than 3. Similarly, the k^{th} AHCs of cogging torque would be introduced when DE exists independently. The results are in agreement with the conculsion of [10]. Thus, the SE and DE could be regarded as two special cases of ME.

B. COGGING TORQUE UNDER MANUFACTURING TOLERANCES

When there are random manufacturing tolerances in rotor PM poles and stator teeth, as shown in Fig.4, i.e., the G_i of every PM pole and the Γ_i of every tooth may differ. As indicated in (6), the n and k can be any positive integer in this case.

Subsequently, ignoring rotor eccentricity, by substituting the new n and k into (4), AHCs of cogging torque would be introduced. Specifically, when stator tolerances are present only, the Λ^2 would exhibit harmonics of $2ip$ orders. These harmonics, in conjunction with the corresponding F_r^2 harmonics, would result in $\mathbb{B}$ in (10) being non-zero, thereby generating additional $2ip^{th}$ AHCs of cogging torque. Similarly, when rotor PM tolerances are present only, AHCs with the orders of iQ_s would arise in cogging torque.

TABLE 3. The possible extra AHCs of cogging torque under ME with the manufacturing tolerances.

Tolerance	Harmonics without ME	Harmonics with ME
Stator tolerances	$2ip$	$2ip$, $2ip\pm1$, $2ip\pm2$, ...
Rotor tolerances	iQ_s	iQ_s, $iQ_s\pm1$, $iQ_s\pm2$, ...
Both	$2ip$, iQ_s	$2ip$, $2ip\pm1$, $2ip\pm2$, iQ_s, $iQ_s\pm1$, $iQ_s\pm2$, ...

Considering tooth and PM tolerances simultaneously, due to the arbitrariness of the values of n and k, AHCs of cogging torque with any orders might be introduced. However, in practice, stator and rotor tolerances primarily cause low-order additional harmonics, which have minimal impact on the main harmonics of F_r^2 and Λ^2. Hence, only considerating the interaction of additional Λ^2 harmonics with inherent $2ip^{th}$ F_r^2 harmonics and the interaction of additional F_r^2 harmonics with inherent $iQ_s{}^{th}$ Λ^2 harmonics is sufficient. In other words, it can be assumed that the effects of stator and rotor tolerances on cogging torque are independent of each other and the case of coexistence of stator and rotor tolerances can be considered as the combination of stator and rotor tolerances.

C. COGGING TORQUE UNDER BOTH ME AND MANUFACTURING TOLERANCES

When there are both ME and random tolerances, AHCs of cogging torque would be introduced because $\mathbb{ABCDE}$ in (10) may be all non-zero. While the 1^{st} cogging torque harmonics caused by $\mathbb{A}$ also can be ignored and harmonics caused by $\mathbb{B}$ are the same as the case only manufacturing tolerances existing, i.e., harmonics with orders of $2ip$ and iQ_s.

On the other hand, as mentioned above, only the interaction of additional Λ^2 harmonics with inherent rotor MMF harmonics and the interaction of additional F_r^2 harmonics with inherent air-gap permeance harmonics being considered in tolerances analysis is sufficient. Therefore, the $\mathbb{C}$ and $\mathbb{D}$ can be neglected, though, theoretically, $\mu_2{}^{th}$ AHCs of cogging torque might arise due to $\mathbb{C}$ and $(\mu_1 \pm \mu_2)^{th}$ AHCs of cogging torque might arise due to $\mathbb{D}$. Hence, only AHCs caused by $\mathbb{E}$ are discussed below.

Firstly, only tooth tolerances are considered. When $k = 2ip \pm \mu_1$, the corresponding $(2ip \pm \mu_2)^{th}$ AHCs of cogging torque arise. The corresponding relationship between μ_1 and μ_2 are listed in Table 1, which will not be reiterated here and below. Hence, in addition to the AHCs of cogging torque

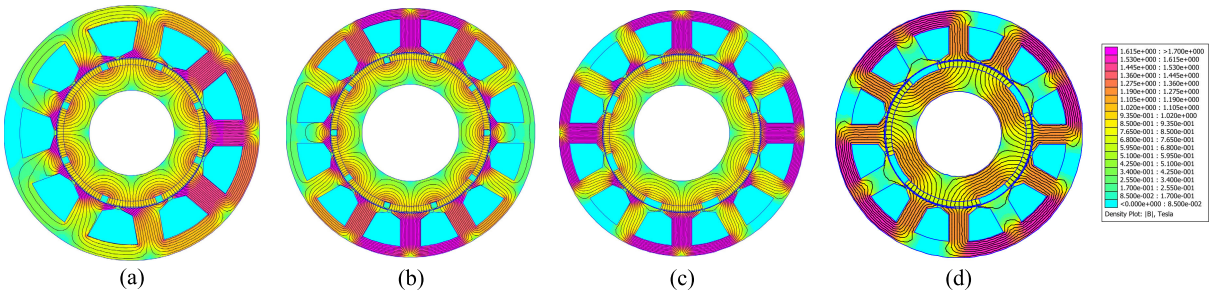

FIGURE 5. Models of SPM with different pole/slot combinations: (a)8P9S; (b)10P12S; (c)8P12S.

TABLE 4. Main parameters of different motors.

Pole/slot	8/9	10/12	8/12	4/12
Stator outer diameter (mm)	180			
Stator inner diameter (mm)	106.2	116.2	116.2	108.2
Rotor outer diameter (mm)	104.2	114.2	114.2	106.2
Shaft outer diameter (mm)	60	70	70	62
Active length (mm)	144			
Stator tooth width (mm)	18.9	14.9	14.9	14.9
Stator yoke height (mm)	11.3	7.6	7.6	11.5
Slot openning width (mm)	3			
Pole-arc ratio	0.86	0.88	0.70	0.72
Magnet remanence (T)	1.2			
Magnet thickness (mm)	4			
Magnetization	Radial			

introduced by ME shown in Table 2, the $2ip^{th}$, $(2ip\pm1)^{th}$, and $(2ip\pm2)^{th}$ AHCs would be further induced in this case.

Secondly, only PM tolerances are considered. When $n = iQ_s \pm \mu_1$, the corresponding $(iQ_s \pm \mu_1 \pm \mu_2)^{th}$ AHCs of cogging torque appear. Hence, in this case, AHCs might be further introduced with the orders of iQ_s, $(iQ_s\pm1)^{th}$, $(iQ_s\pm2)^{th}$, and so on.

Finally, tooth and PM tolerances are considered simultaneously. Same as the case of only considering manufacturing tolerances, it can be simply assumed that the AHCs of cogging torque are the superposition of the AHCs when the stator and rotor are separate.

In summary, excluding the inherent and ME introduced harmonic components of cogging torque (shown in Table 2), the possible extra AHCs of cogging torque with the coexistence of stator or rotor tolerances are listed in Table 3.

IV. QUANTITATIVE ANALYSIS OF COGGING TORQUE VIA FEM

A. COGGING TORQUE UNDER ME

To verify the influence mechanism of ME on cogging torque, an 8P9S surface-mounted PM (SPM) motor, with $n = 8i$, $k = 9i$, and $72i^{th}$ inherent cogging torque harmonics, is taken as an example. The structure of the model is shown in Fig.5(a) and the main parameters are listed in Table 4. The purpose of the models in this paper is to verify the influence mechanism of manufacturing uncertainties, so the parameters are not optimal.

Based on Table 2, primarily, the $(72i\pm1)^{th}$ exist as the inherent AHCs of cogging torque. Then the AHCs of 8^{th} and 9^{th} ($n = 8, k = 9$), 16^{th} and 18^{th} ($n = 16, k = 18$), 24^{th} and 27^{th} ($n = 24, k = 27$), 45^{th} and 48^{th} ($n = 48, k = 45$), 54^{th} and 56^{th} ($n = 56, k = 54$), etc. are introduced similar with the SE and DE cases. Accordingly, the presence of the 7^{th} and 10^{th} AHCs are attributed to $(\mu_1, \mu_2)\in$ {(1,-1), (1,2)}, corresponding to the second row of Table 2. And the existence of the 17^{th} and 55^{th} AHCs are due to $(\mu_1, \mu_2) = (2,1)$, corresponding to the third row of Table 2. Additionally, the 25^{th}, 26^{th}, 46^{th}, and 47^{th} AHCs exist when $(\mu_1, \mu_2)\in$ {(3,1), (3,2)}, corresponding to the fourth row of Table 2. Setting $\epsilon_1 = \epsilon_2 = 0.25$, partial cogging torque harmonics calculated by FEM are shown in Fig. 6(a). Due to the relatively large amplitude of the inherent 72^{th} harmonic component of cogging torque, it is interrupted to show. And the grey scale characterizes the torque range from the break to the upper edge of the bar graph.

As can be observed from Fig. 6(a), the AHCs of cogging torque are coincident with the theoretical analysis above, as previously predicted. However, the amplitudes of AHCs introduced due to $(\mu_1, \mu_2)\in$ {(1,-1), (1,2), (3,1), (3,2)} are very small. Because the components of MEC casuing these AHCs of cogging torque are produced by the products of $D_s(1)$ and $D_r(2)$, as well as $D_r(1)$ and $D_s(2)$ according to (8), and the amplitudes of $D_s(2)$ and $D_r(2)$ are relatively small as depicted in Fig. 3. Moreover, the $72[= LCM(8, 9)]^{nd}$ harmonic is the inherent cogging torque harmonic of 8P9S motor, which is not the emphasis of this paper (similiar with other $LCM(n, k)^{th}$ cogging torque harmonics of different pole/slot configurations).

Further, the cogging torque harmonics of the 10P12S, 8P12S and 4P12S SPM motors under ME with $\epsilon_1 = \epsilon_2 = 0.25$ are also calculated by FEM. The 10P12S and 8P12S SPM motors are fractional slot motors, while the 4P12S SPM motor is a example of integer slot motors. The structures of their models are shown in Fig.5(b)-(d) and the results are reported in Fig. 6(b)-(d).

Notably, there are 1^{st} AHCs of cogging torque in Fig. 6(b)-(d), which are introduced because $\mathbb{A}$ in (10).

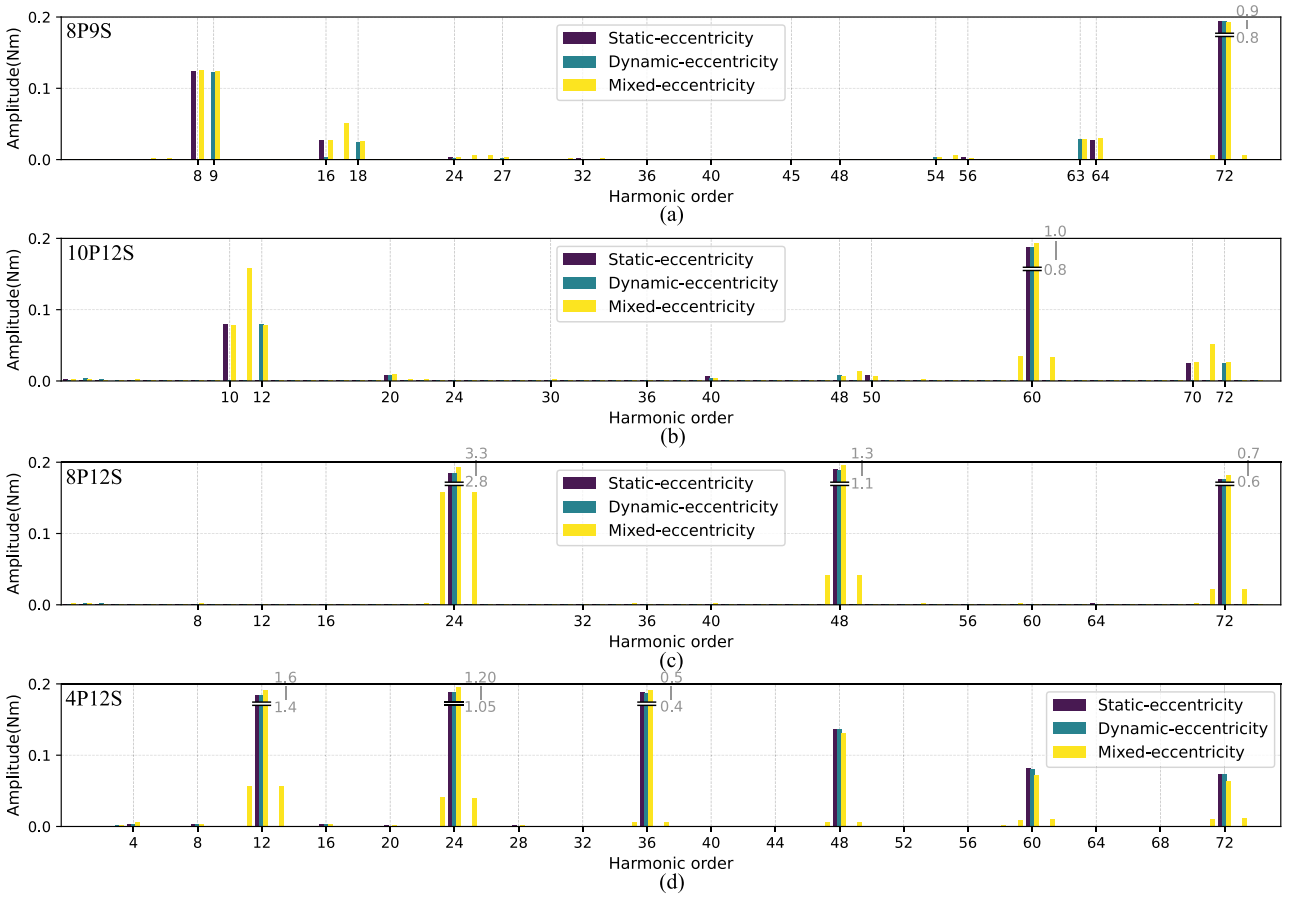

FIGURE 6. Partial cogging torque harmonics of PM motors with different pole/slot configurations under ME: (a)8P9S; (b)10P12S; (c)8P12S; (d)4P12S.

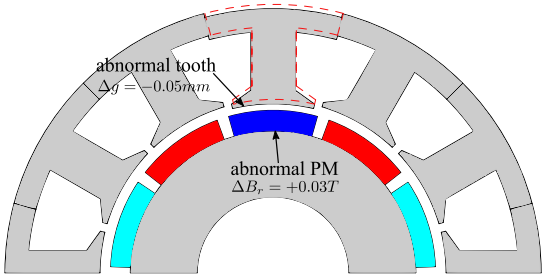

FIGURE 7. The schematic diagram of typical manufacturing tolerances.

However, their amplitudes are so small that it is reasonable to ignore the influence of $\mathbb{A}$ in the ME analysis. Beyond the 1^{st} AHC, all harmonics in Fig. 6 can be explained theoretically combined with Table 2, which proves the efficacy of MEC and the efficiency of Table 2 in the process of analysis of AHCs under ME.

B. COGGING TORQUE UNDER BOTH ME AND MANUFACTURING TOLERANCES

The 8P9S PM motor is also taken as an example to illustrate the possible harmonics of cogging torque under ME with the existence of stator or rotor tolerances. According to Table 3, excluding the AHCs of cogging torque caused by the independent influence of ME, the coexistence of ME and tooth tolerances mainly introduce $8i^{th}$, $(8i\pm1)^{th}$, $(8i\pm2)^{th}$ AHCs. While the coexistence of ME and PM tolerances mainly introduce $9i^{th}$, $(9i\pm1)^{th}$, $(9i\pm2)^{th}$ AHCs. Furthermore, when ME coexists with stator and rotor tolerances, all of these AHCs mentioned above would be present. And it can be seen as the coupling effect of rotor eccentricity and manufacturing tolerances on the harmonic components of cogging torque.

As shown in Fig.7, one single abnormal tooth with the inner diameter tolerance of $\Delta g = -0.05$mm and one single abnormal PM with the remanence tolerance of $\Delta B_r = +0.03$T are considered as the representatives of stator and rotor tolerances, respectively. The harmonic components of cogging torque of the 8P9S PM motor under these tolerances without and with ME ($\epsilon_1 = \epsilon_2 = 0.25$) are calculated by FEM and the results are shown in Fig. 8(a)(b).

It can be observed from Fig. 8 that the aforementioned AHCs of cogging torque introduced in the model with ME compared to without ME are in accordance with Table 3, except harmonic components whose orders are low. These lower-order harmonics are the $\mu_2{}^{th}$ and $(\mu_1 \pm \mu_2)^{th}$ AHCs of cogging torque due to $\mathbb{C}$ and $\mathbb{D}$, respectively. As discussed in the Section III Part C, these AHCs could be ignored since

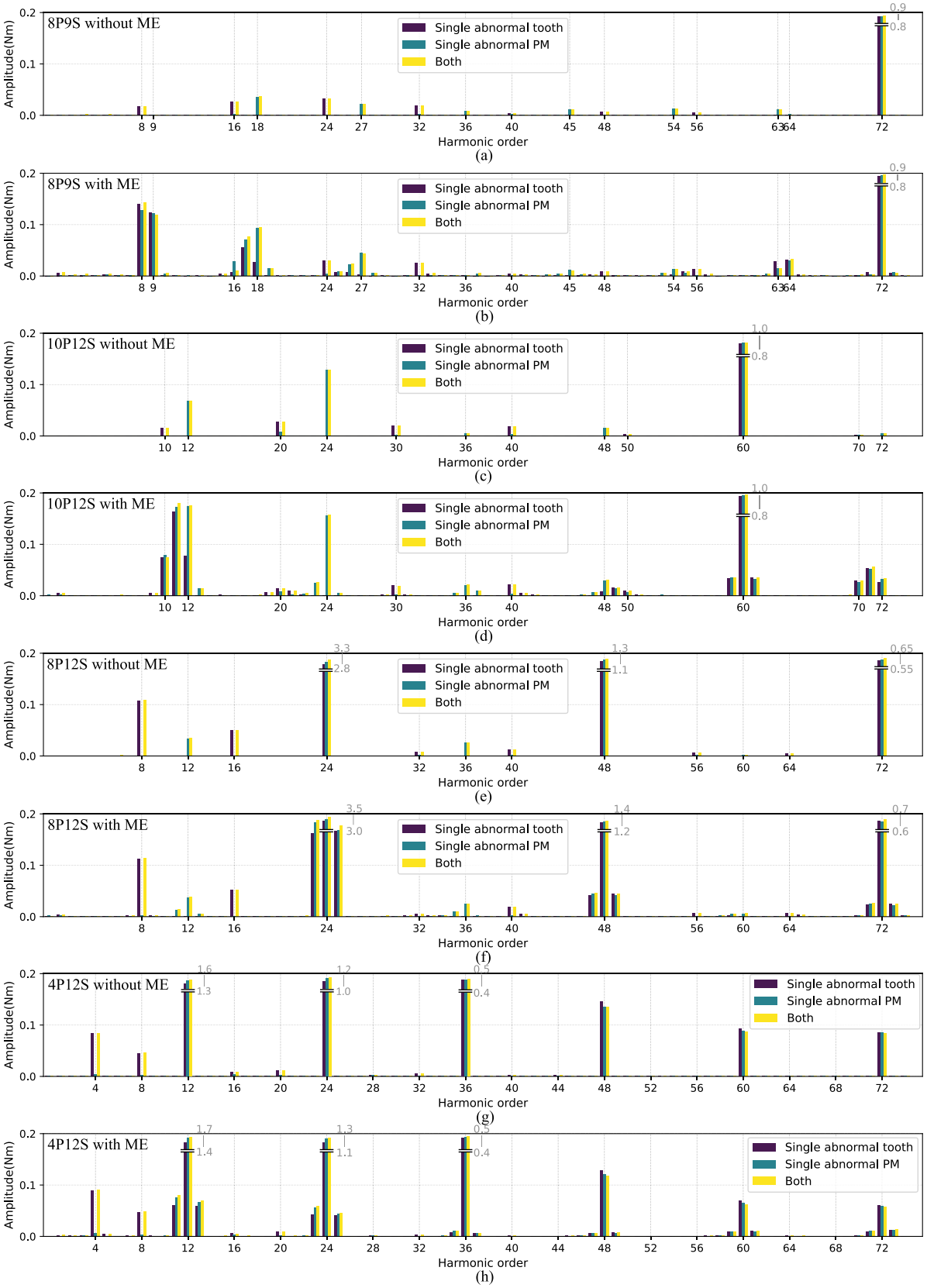

FIGURE 8. Partial cogging torque harmonics of PM motors with different pole/slot configurations with manufacturing tolerances: (a)8P9S without ME; (b)8P9S with ME; (c)10P12S without ME; (d)10P12S with ME; (e)8P12S without ME; (f)8P12S with ME; (g)4P12S without ME; (h)4P12S with ME.

they are caused by the lower-order F_r^2 and Λ^2. The FEM results also indicate that the amplitudes of these harmonics are relatively smaller compared to other AHCs, and their frequencies are not significantly high. Consequently, it can be inferred that their influence on the cogging torque is negligible.

Therefore, combining the results of theoretical analysis and FEM, it can be concluded that the main AHCs of cogging torque under ME with stator and rotor tolerances simultaneously are the terms of $2ip^{th}$, $(2ip\pm1)^{th}$, iQ_s^{th}, and $(iQ_s\pm1)^{th}$, excluding the cogging torque harmonics introduced by the inherent pole/slot configuration and only ME.

Similarly, the 10P12S, 8S12P and 4P12S SPM motors are also calculated by FEM in the same condition of ME and manufacturing tolerances, and their results are reported in Fig. 8(c)-(h). The main AHCs of cogging torque are consistent with the analysis results, proving the validity of the proposed analytical model and analysis conclusion.

V. METHODS TO REDUCE THE INFLUENCE OF MANUFACTURING UNCERTAINTIES

Improving manufacturing and assembly precision to control the ranges of uncertainties is a direct way to prevent the deterioration of cogging torque in actual motors. However, the improvement of precision would result in a significant increase in manufacturing costs. In this section, some instructions on how to reduce the influence of manufacturing uncertainties based on the pole-arc selection are discussed.

A. SELECTION OF DIFFERENT POLE/SLOT COMBINATIONS

According to (10) and Table 1, as for a PM motor with a specific pole/slot combination under rotor eccentricity, the condition of $(n-k\pm\mu_1)=0$ is hard to achieve when its values of n and k are no less than 3. Moreover, the AHCs of cogging torque under ME with lower orders have larger amplitudes. The AHCs with $2p$ order, Q_s order, and orders near them are more significant. Namely, if the difference between the number of poles and the number of slots in a PM motor, there is a significant impact of ME on the cogging torque.

As shown in Fig. 6, almost no AHCs of cogging torque except the $(24i\pm1)^{th}$ and $(12i\pm1)^{th}$ inherent AHCs are introduced in 8P12S and 4P12S configurations. While there are more AHCs with lower orders (relative to inherent harmonics) in 8P9S and 10P12S configurations.

Moreover, two-cycle cogging torque waveforms of all configurations under both single abnormal tooth and PM without/with ME are shown in Fig. 9. It can be observed that the larger the difference value of $2p$ and Q_s is, the less difference of cogging torque waves of different cases, such as 8P12S and 4P12S configurations. Therefore, it can be summarized that the PM motor with a similar number of poles and slots is more sensitive to rotor eccentricity than other pole/slot configurations.

However, there is more serious cogging torque in the ideal condition when the difference of $2p$ and Q_s is large. Because the inherent cogging torque harmonics have lower orders and larger amplitudes if no cogging torque suppression measures are taken. Therefore, the final determination of pole/slot combination in the design step is a process of trade-off between robustness under manufacturing uncertainties and inherent performance of cogging torque. Therefore, the final determination of pole/slot combination in the design step is a process of trade-off between robustness under manufacturing uncertainties and inherent performance of cogging torque. While ensuring that the nominal cogging torque is not excessive, it is advisable to select a configuration with a slightly larger difference in the number of poles and teeth.

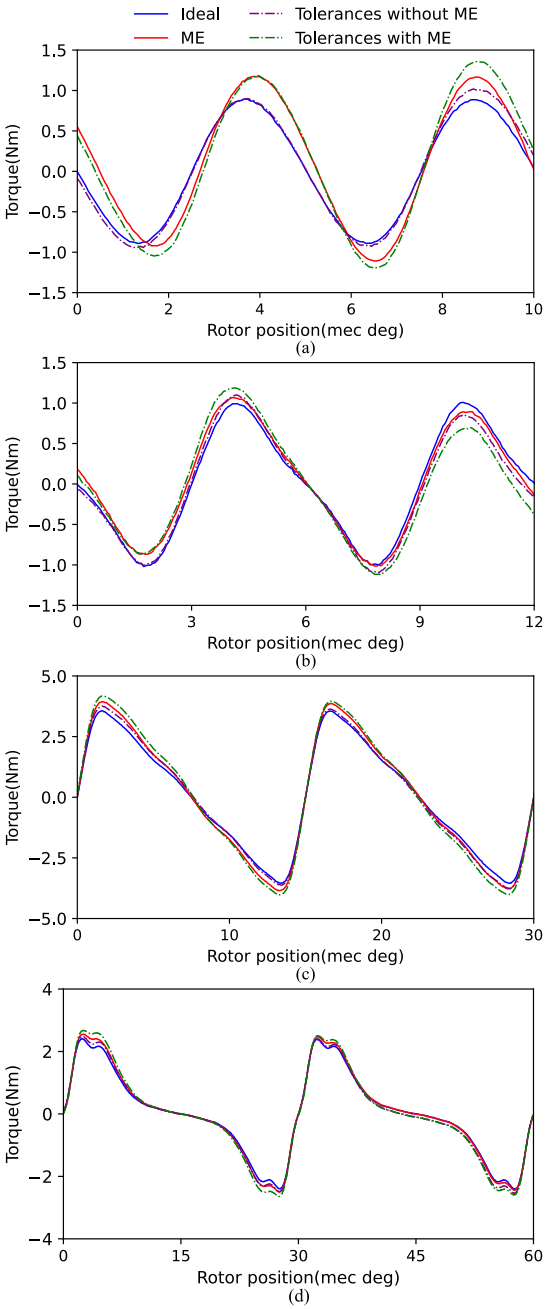

FIGURE 9. Cogging torque waves of PM motors with different pole/slot configurations under ME: (a)8P9S; (b)10P12S; (c)8P12S; (d)4P12S.

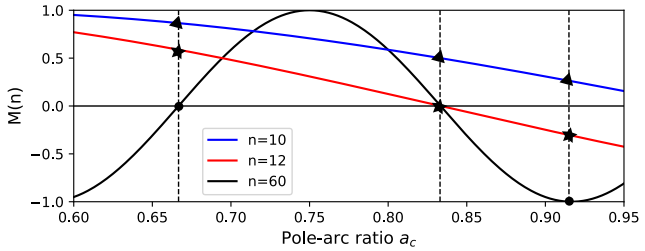

FIGURE 10. The variation of $M(n)$ at different a_c.

B. DESIGN OF POLE-ARC RATIO

Based on the results of analysis, the most significant AHCs, which have relatively larger amplitudes, of cogging torque introduced by manufacturing uncertainties are $2p^{th}$, Q_s^{th}, and harmonic components of orders between $2p$ and Q_s (existing under ME only).

According to the $\mathbb{B}$ in (10), the $2p^{th}$ and Q_s^{th} AHCs of cogging torque under manufacturing tolerances are introduced by the interaction of the same order of F_r^2 harmonic and Λ^2 harmonic. Specifically, $2p^{th}$ AHC is introduced by the interaction of $2p^{th}$ F_r^2 and $2p^{th}$ Λ^2, while $Q_s{}^{th}$ AHC is introduced by the interaction of $Q_s{}^{th}$ F_r^2 and $Q_s{}^{th}$ Λ^2. The $2p^{th}$ Λ^2 and $Q_s{}^{th}$ F_r^2 are caused by stator tolerances and PM tolerances, respectively.

On the other hand, according to the $\mathbb{E}$ in (10), the main AHCs of cogging torque under ME in the same row of Table 2 are introduced by the interaction of the same order of F_r^2 harmonic and the same order of Λ^2 harmonic with different harmonics of MEC. For example, as for the cell in "$|n-k| = 2$" row and "$n < k$" column, the n^{th} and k^{th} AHCs are introduced by the n^{th} F_r^2 and k^{th} Λ^2 with $D_m(2,0)\cos(2\theta)$ and $D_m(2,2)\cos(2\theta-2\theta)$, respectively. While the $(n+1)^{th}$ AHC is introduced by the n^{th} F_r^2 and k^{th} Λ^2 with $D_m(2,1)\cos(2\theta-\theta)$. Therefore, the dominant AHCs of cogging torque under rotor eccentricity are all introduced by the interaction of $2p^{th}$ F_r^2 and $Q_s{}^{th}$ Λ^2.

In a nutshell, as for the MMF of PMs, the $2p^{th}$ F_r^2 and $Q_s{}^{th}$ F_r^2 are the main causes of AHCs of cogging torque under manufacturing uncertainties, and the influence of manufacturing uncertainties could be eliminated by reducing them.

As shown in (6), the relationships between the amplitudes of n^{th} F_r^2 and the parameters of the PM motor itself are:

$$G(n) \propto \left|\sin\frac{n\pi a_c}{2p}\right|. \tag{11}$$

The $\sin[n\pi a_c/2p]$ is defined as $M(n)$. As observed from (11), the influence of manufacturing uncertainties on cogging torque can be eliminated with proper selections of the pole-arc ratio a_c to make $M(2p)$ and $M(Q_s)$ set to zero.

Moreover, the dominantly inherent harmonic component of cogging torque is $LCM(2p, Q_s)^{th}$, which is introduced by the interaction of $LCM(2p, Q_s)^{th}$ F_r^2 and $LCM(2p, Q_s)^{th}$ Λ^2.

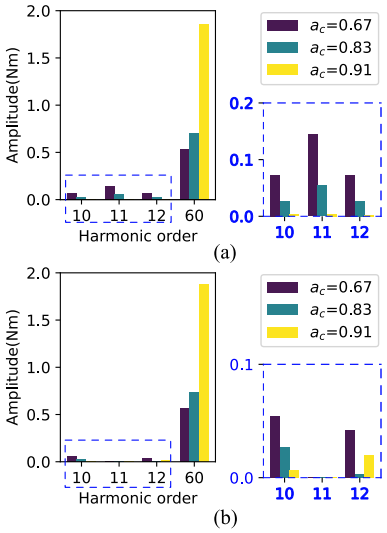

FIGURE 11. The variation of AHCs of cogging torque at different a_c: (a)under ME; (b)under manufacturing tolerances.

Therefore, a superior design of PM motor with small cogging torque and high robustness against rotor eccentricity could be obtained by properly selecting a_c to make $|M[LCM(2p, Q_s)]|$, $|M(2p)|$, and $|M(Q_s)|$ as small as possible simultaneously. The first one affects the nominal performance of cogging torque, while the robustness of cogging torque against rotor eccentricity and stator tolerances is influenced by the middle one and the robustness against PM tolerances is influenced by the last one.

The 12S10P configuration is selected as an example. Based on (10), the dominant AHCs introduced by manufacturing tolerances are 10^{th} and 12^{th} which are caused by 10^{th} and 12^{th} F_r^2, respectively. The dominant AHCs introduced by ME are 10^{th}, 11^{th}, and 12^{th} which are all caused by the 10^{th} F_r^2, respectively. While the dominant inherent harmonic of cogging torque is 60^{th} which is caused by 60^{th} F_r^2. Therefore, a relatively excellent and more robust design of it should have a small value of $|M(10)|$, $|M(12)|$, and $|M(60)|$. Based on (11), the variations of their values with several different a_c are shown in Fig. 10.

Because a_c is usually selected within the range of (0.6,0.95) [17], only designs belonging to this range are considered. As can be observed from Fig. 10, the $|M(60)|$ is at peak value when a_c is equal to 0.67 and 0.83, while it is zero when a_c is equal to 0.91. It means that the 60^{th} harmonic, that is the nominal performance, of cogging torque is minimum when a_c is equal to 0.67 and 0.83. However, the values of $|M(10)|$ and $|M(12)|$ are smaller at $a_c = 0.83$ than 0.67. It means that the 10^{th} and 12^{th} harmonics introduced by manufacturing uncertainties are smaller, that is the robustness against manufacturing uncertainties is better, when a_c is equal to 0.83. Therefore, the design of 10P12S with $a_c = 0.83$ is prior based on the theoretical analysis.

Moreover, it is worth noting that the $|M(10)|$ is smaller at $a_c = 0.91$ than 0.83. It means that the 10^{th} and 12^{th} harmonics

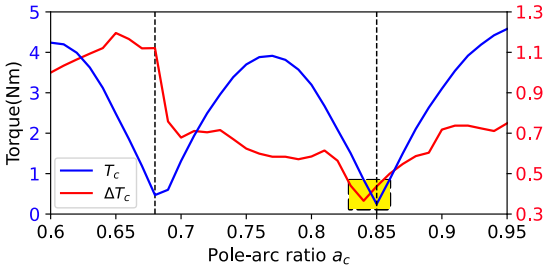

FIGURE 12. The variation of the peak-to-peak values of cogging torque at different a_c.

of cogging torque introduced by rotor eccentricity, that is the robustness against rotor eccentricity, is better when a_c is equal to 0.91, though the nominal cogging torque is inferior.

The variations of 10^{th}, 12^{th}, and 60^{th} harmonics of cogging torque with different a_c under ME ($\epsilon_1 = \epsilon_2 = 0.25$) or manufacturing tolerances [one single abnormal PM ($\Delta B_r = +0.03$T), and one single abnormal slot($\Delta g = -0.05$mm)] are calculated via FEM to verify the analysis results. The results are shown in Fig. 11.

As shown in Fig. 11(a), the amplitudes of 10^{th}, 11^{th}, and 12^{th} AHCs synchronously decrease with the enlargement of a_c under ME. And the amplitude of 60^{th} harmonic of cogging torque at $a_c = 0.91$ is significantly larger than the other two. Their trends of change are consistent with the $M(10)$ and $M(60)$ in Fig. 10.

As shown in Fig. 11(b), the amplitude of 10^{th} AHC decreases with the enlargement of a_c under manufacturing tolerances, while the amplitude of 12^{th} AHC at $a_c = 0.83$ is significantly smaller than other two. Their trends of change are consistent with the $M(10)$ and $M(12)$ in Fig. 10.

The above simulation results demonstrate the correctness of the mechanism of cogging torque AHCs and the effectiveness of selecting pole-arc ratio to reduce the specific harmonic.

The difference between the peak-to-peak values of cogging torque at the case of all proposed uncertainties (both ME and manufacturing tolerances) and the ideal case is also calculated and represented by ΔT_c. T_c (the peak-to-peak values of cogging torque at the ideal case) and ΔT_c of the 10P12S motor with different a_c are shown in Fig. 12.

As shown in Fig. 12, the variation of T_c is consistent with $|M(60)|$ (or the amplitude of the 60^{th} F_r^2). And the ΔT_c of the design with $a_c \approx 0.83$ is the smallest, which is consistent with $|M(10)|$ and $|M(12)|$ (or the amplitude of the 10^{th} and 12^{th} F_r^2).

The a_c in the actual motor is slightly bigger than the theoretical value of 0.83 in Fig. 12, which results from the influence of flux leakage. Therefore, the designs within the yellow area (with $a_c \approx 0.84$) can be selected in the specific design. These designs are not only relatively optimal but also robust. The simulation results demonstrate the effectiveness of determining the optimal pole-arc ratio to reduce the nominal cogging torque and the influence of manufacturing uncertainties simultaneously based on theoretical analysis, which can provide convenient guidance for robust design and optimization of cogging torque in PM motors.

VI. CONCLUSION

In this paper, an investigation of the influence of ME without/with manufacturing tolerances on the cogging torque of PM motors is presented by a modified analytical model with MEC. And its efficacy is verified by calculations on several SPM motors having different pole/slot configurations via FEM. It shows that the influence of ME on air-gap can be recognized as the product of the independent effects of SE and DE. Subsequently, various AHCs of cogging torque would be introduced in PM motors under ME when there is $|2i_1p - i_2Q_s| \leq 3$. Moreover, considering the coexistence of ME and manufacturing tolerances, significant emphasis should also be put on the $2ip^{th}$, $(2ip\pm1)^{th}$, iQ_s^{th}, and $(iQ_s\pm1)^{th}$ extra AHCs of cogging torque. Based on the conclusion, the theoretical reference for the selection of pole/slot configurations and the method for robust design by selecting a proper pole-arc ratio to reduce the specific AHCs introduced by manufacturing uncertainties are proposed.

REFERENCES

[1] T. Orlowska-Kowalska, M. Wolkiewicz, P. Pietrzak, M. Skowron, P. Ewert, G. Tarchala, M. Krzysztofiak, and C. T. Kowalski, "Fault diagnosis and fault-tolerant control of PMSM drives–state of the art and future challenges," *IEEE Access*, vol. 10, pp. 59979–60024, 2022.

[2] H. Y. Sun and K. Wang, "Effect of third harmonic flux density on cogging torque in surface-mounted permanent magnet machines," *IEEE Trans. Ind. Electron.*, vol. 66, no. 8, pp. 6150–6158, Aug. 2019.

[3] Y. Yang, X. Wang, R. Zhang, T. Ding, and R. Tang, "The optimization of pole arc coefficient to reduce cogging torque in surface-mounted permanent magnet motors," *IEEE Trans. Magn.*, vol. 42, no. 4, pp. 1135–1138, Apr. 2006.

[4] H. Zhuang, S. Zuo, Z. Ma, Q. Yu, Z. Wu, and C. Liu, "Magnetic analysis of skew effect in surface-mounted permanent magnet machines with skewed slots," *IEEE Trans. Magn.*, vol. 58, no. 12, pp. 1–12, Dec. 2022.

[5] F. Liu, X. Wang, Z. Xing, A. Yu, and C. Li, "Reduction of cogging torque and electromagnetic vibration based on different combination of pole arc coefficient for interior permanent magnet synchronous machine," *CES Trans. Electr. Mach. Syst.*, vol. 5, no. 4, pp. 291–300, Dec. 2021.

[6] J. Qu, J. Jatskevich, C. Zhang, and S. Zhang, "Torque ripple reduction method for permanent magnet synchronous machine drives with novel harmonic current control," *IEEE Trans. Energy Convers.*, vol. 36, no. 3, pp. 2502–2513, Sep. 2021.

[7] Y. Li, Q. Lu, Z. Q. Zhu, L. J. Wu, G. J. Li, and D. Wu, "Analytical synthesis of air-gap field distribution in permanent magnet machines with rotor eccentricity by superposition method," *IEEE Trans. Magn.*, vol. 51, no. 11, pp. 1–4, Nov. 2015.

[8] J. Ou, Y. Liu, R. Qu, and M. Doppelbauer, "Experimental and theoretical research on cogging torque of PM synchronous motors considering manufacturing tolerances," *IEEE Trans. Ind. Electron.*, vol. 65, no. 5, pp. 3772–3783, May 2018.

[9] S.-G. Lee, S. Kim, J.-C. Park, M.-R. Park, T. H. Lee, and M.-S. Lim, "Robust design optimization of SPMSM for robotic actuator considering assembly imperfection of segmented stator core," *IEEE Trans. Energy Convers.*, vol. 35, no. 4, pp. 2076–2085, Dec. 2020.

[10] Z. Q. Zhu, L. J. Wu, and M. L. Mohd Jamil, "Influence of pole and slot number combinations on cogging torque in permanent-magnet machines with static and rotating eccentricities," *IEEE Trans. Ind. Appl.*, vol. 50, no. 5, pp. 3265–3277, Sep. 2014.

[11] H. Qian, H. Guo, Z. Wu, and X. Ding, "Analytical solution for cogging torque in surface-mounted permanent-magnet motors with magnet imperfections and rotor eccentricity," *IEEE Trans. Magn.*, vol. 50, no. 8, pp. 1–15, Aug. 2014.

[12] W. Tong, S. Li, X. Pan, S. Wu, and R. Tang, "Analytical model for cogging torque calculation in surface-mounted permanent magnet motors with rotor eccentricity and magnet defects," *IEEE Trans. Energy Convers.*, vol. 35, no. 4, pp. 2191–2200, Dec. 2020.
[13] B. M. Ebrahimi, J. Faiz, and M. J. Roshtkhari, "Static-, dynamic-, and mixed-eccentricity fault diagnoses in permanent-magnet synchronous motors," *IEEE Trans. Ind. Electron.*, vol. 56, no. 11, pp. 4727–4739, Nov. 2009.
[14] S. Jia, R. Qu, J. Li, Z. Fu, H. Chen, and L. Wu, "Analysis of FSCW SPM servo motor with static, dynamic and mixed eccentricity in aspects of radial force and vibration," in *Proc. IEEE Energy Convers. Congr. Expo. (ECCE)*, Sep. 2014, pp. 1745–1753.
[15] R. S. C. Pal and A. R. Mohanty, "A simplified dynamical model of mixed eccentricity fault in a three-phase induction motor," *IEEE Trans. Ind. Electron.*, vol. 68, no. 5, pp. 4341–4350, May 2021.
[16] C. Ma, J. Li, N. Zhang, F. Bu, and Z. Yang, "Open-circuit radial stray magnetic flux density based noninvasive diagnosis for mixed eccentricity parameters of interior permanent magnet synchronous motors in electric vehicles," *IEEE Trans. Ind. Electron.*, vol. 70, no. 2, pp. 1983–1992, Feb. 2023.
[17] Y. Yang, N. Bianchi, G. Bramerdorfer, C. Zhang, and S. Zhang, "Methods to improve the cogging torque robustness under manufacturing tolerances for the permanent magnet synchronous machine," *IEEE Trans. Energy Convers.*, vol. 36, no. 3, pp. 2152–2162, Sep. 2021.
[18] U. Galfarsoro, A. McCloskey, S. Zarate, X. Hernández, and G. Almandoz, "Influence of manufacturing tolerances and eccentricities on the unbalanced magnetic pull in permanent magnet synchronous motors," *IEEE Trans. Ind. Appl.*, vol. 58, no. 3, pp. 3497–3510, May 2022.
[19] J. Pu, W. Xiuhe, and W. Daohan, "Study of cogging torque in surface-mounted permanent magnet motors with static eccentricity," *Proc. CSEE*, vol. 24, no. 9, pp. 188–191, 2004.
[20] W. Sun, H. Wang, and R. Qu, "A novel data generation and quantitative characterization method of motor static eccentricity with adversarial network," *IEEE Trans. Power Electron.*, vol. 38, no. 7, pp. 8027–8032, Apr. 2023.
[21] Y. Yang, N. Bianchi, C. Zhang, X. Zhu, H. Liu, and S. Zhang, "A method for evaluating the worst-case cogging torque under manufacturing uncertainties," *IEEE Trans. Energy Convers.*, vol. 35, no. 4, pp. 1837–1848, Dec. 2020.
[22] T. R. He, Z. Q. Zhu, F. Xu, Y. Wang, H. Bin, and L. M. Gong, "Influence of rotor eccentricity on electromagnetic performance of 2-pole/3-slot PM motors," *IEEE Trans. Energy Convers.*, vol. 37, no. 1, pp. 696–706, Mar. 2022.

YUE ZHAO received the bachelor's degree in vehicle engineering from Shijiazhuang Tiedao University, in 2018. He is currently pursuing the Ph.D. degree with the Beijing Institute of Technology.

His research interests include robust design and optimization on electrical machines and cogging torque analysis considering manufacturing tolerances.

SHUO ZHANG (Member, IEEE) received the B.Eng. degree from the North China Institute of Aerospace Engineering, Hebei, China, in 2011, and the Ph.D. degree in vehicle engineering from the Beijing Institute of Technology, Beijing, China, in 2017.

He is currently an Associate Professor with the National Engineering Laboratory for Electric Vehicles and the School of Mechanical Engineering, Beijing Institute of Technology. His research interests include the modeling and control of the permanent magnet synchronous motor, multi-motor driving systems, and hybrid power systems.

CHENGNING ZHANG received the M.E. degree in control theory and control engineering and the Ph.D. degree in vehicle engineering from the Beijing Institute of Technology, Beijing, China, in 1989 and 2001, respectively.

He is currently a Professor and the Vice Director of the National Engineering Laboratory for Electric Vehicles, Beijing Institute of Technology. His research interests include electric vehicles, vehicular electric motor drive systems, battery management systems, and chargers.

GUOHUI YANG received the B.Eng. degree in vehicle engineering from the Hefei University of Technology, Hefei, China, in 2016, and the Ph.D. degree in mechanical engineering from the Beijing Institute of Technology, Beijing, China, in 2022.

He has been with the Laboratory of Aerospace Servo Actuation and Transmission (LASAT), Beijing Institute of Precision Mechatronics and Controls, since 2022. His research interests include the servo system design for launch vehicles, thermal analysis and optimization of PM servo machines.

YONGXI YANG received the B.Eng. and Ph.D. degrees in vehicle engineering from the Beijing Institute of Technology, Beijing, China, in 2014 and 2021, respectively.

He is currently an Assistant Professor with the National Engineering Laboratory for Electric Vehicles, Beijing Institute of Technology. His research interests include the robust design and optimization of PM machines with considerations of the effects of manufacturing tolerances.